# $^{17}O$ and $^{1}H$ relaxometric and DFT study of hyperfine coupling constants in $[Mn(H_2O)_6]^{2+}$ [i]

David Esteban-Gómez[a], Claudio Cassino[b], Mauro Botta[b] and Carlos Platas-Iglesias[a*]

[a] Departamento de Química Fundamental, Universidade da Coruña, Rúa da Fraga 10, A Coruña, Spain

[b] Dipartimento di Scienze e Innovazione Tecnologica, Università del Piemonte Orientale "Amedeo Avogadro", Viale T. Michel 11, Alessandria, Italy

**RSC Advances**, volume 4, issue 14, pages 7094–7103
Received 10 October 2013, accepted 02 January 2014, first published 06 January 2014

**How to cite:** $^{17}O$ and $^{1}H$ relaxometric and DFT study of hyperfine coupling constants in $[Mn(H_2O)_6]^{2+}$. D. Esteban-Gómez, C. Cassino, M. Botta and C. Platas-Iglesias, *RSC Adv.*, 2014, 7094–7103. DOI: 10.1039/C3RA45721D.

## Abstract

Nuclear Magnetic Relaxation Dispersion (NMRD) profiles and $^{17}O$ NMR chemical shifts and transverse relaxation rates of aqueous solutions of $[Mn(H_2O)_6]^{2+}$ were recorded to determine the parameters governing the relaxivity in this complex and the $^{17}O$ and $^{1}H$ hyperfine coupling constants (HFCCs). The analysis of the NMRD and $^{17}O$ NMR data provided a water exchange rate of $k_{ex}^{298} = 28.2 \times 10^6\ s^{-1}$, and $A_O/\hbar$ and $A_H/\hbar$ hyperfine coupling constants of −34.6 and 5.4 rad $s^{-1}$, respectively. DFT calculations (TPSSh model) performed on the $[Mn(H_2O)_6]^{2+}$ and $[Mn(H_2O)_6]^{2+}\cdot 12H_2O$ systems were used to evaluate theoretically the $^{17}O$ and $^{1}H$ HFCCs responsible for the $^{17}O$ NMR chemical shifts and the scalar contributions to $^{17}O$ and $^{1}H$ NMR relaxation rates. The use of a mixed cluster–continuum approach with the explicit inclusion of second-sphere water molecules is critical for an accurate calculation of HFCCs of coordinated water molecules. The impact of complex dynamics on the calculated HFCCs was evaluated with the use of molecular dynamics simulations within the atom-centered density matrix propagation (ADMP) approach. These molecular dynamics simulations show that the $A_{iso}$ values are critically affected by the distance between the oxygen atom of the coordinated water molecule and the $Mn^{II}$ ion, as well as by the orientation of the water molecule plane with respect to the Mn–O vector. The substantial scalar contribution to relaxivity observed for $[Mn(H_2O)_6]^{2+}$ is related to a combination of a slow water exchange rate and a slow electron spin relaxation.

**Keywords:** relaxivity, hiperfine coupling constants, spin relaxation, molecular dynamics simulations

## Introduction

Hyperfine interactions between nuclear spin and electron spin play a key role in the description of NMR relaxation of ligand nuclei in solutions of paramagnetic species.[1] Electron spin relaxation in paramagnetic systems provides fluctuating magnetic fields, and therefore causes nuclear relaxation. The observed nucleus however does not see the unpaired electron(s) as localized, but rather as spin density distributed throughout space. The presence of spin density at the resonating nucleus is responsible for the so called Fermi contact

* carlos.platas.iglesias@udc.es

mechanism to nuclear relaxation, which depends on the hyperfine coupling constant (HFCC) $A/\hbar$ between the electron spin of the metal ion and the nuclear spin.[2]

Recently, we started a research program devoted to the synthesis and physicochemical characterization of $Mn^{II}$ complexes with potential application as contrast agents in magnetic resonance imaging (MRI).[3–5] Contrast agents are paramagnetic probes that enhance the image contrast by shortening the longitudinal and/or transverse relaxation times of water molecules surrounding the complex.[6] Although most commercially available contrast agents are small $Gd^{III}$ chelates, complexes of the $d^5$ metal ion $Mn^{II}$ with high-spin configuration represent an alternative to the classical $Gd^{III}$-based contrast agents. An important potential advantage of $Mn^{II}$-based contrast agents over the classical $Gd^{III}$-based ones is the lower toxicity of $Mn^{II}$ complexes. Furthermore, high-spin $Mn^{II}$ complexes present relatively high effective magnetic moments and slow electronic relaxation rates.[7]

Contrast agents for MRI typically contain one water molecule coordinated to the paramagnetic metal ion that exchanges rapidly with the bulk water. The efficiency of a contrast agent is often evaluated *in vitro* in terms of its relaxivity, which is defined as the longitudinal relaxation rate enhancement of water proton nuclei per mM concentration of the paramagnetic ion. Relaxivity depends upon a relatively large number of parameters that can hardly be determined by analyzing relaxivity data alone.[6] Indeed, variable temperature $^{17}O$ NMR measurements of chemical shifts and transverse relaxation rates constitute a valuable tool to investigate the parameters influencing relaxivity in MRI CAs.[8,9] $^{17}O$ NMR data provide information on the water exchange kinetics of the complex, and depend on the hyperfine coupling constant $A_O/\hbar$ between the electron spin of the metal ion and the $^{17}O$ nuclear spin. Additionally, the Nuclear Magnetic Relaxation Dispersion (NMRD) profiles recorded for some $Mn^{II}$ complexes such as $[Mn(H_2O)_6]^{2+}$ and $[Mn_2(ENOTA)]$ show an unusual dispersion at about 0.1 MHz attributed to an important scalar contribution to relaxivity, which depends on the hyperfine coupling constant $A_H/\hbar$.[9,10] Thus, a detailed study of the $A_O/\hbar$ and $A_H/\hbar$ HFCCs in $Mn^{II}$ complexes is important for the rational development of MRI contrast agents.

Methods based on Density Functional Theory (DFT) provide a reasonably high accuracy at relatively low computational cost, and therefore represent an attractive tool for the calculation of hyperfine coupling constants (HFCCs) in metal complexes. Different studies have shown that DFT methods provide rather accurate HFCCs of different mononuclear[11] and dinuclear[12] Mn complexes. However, calculations on the $Mn^{II}$ complex with one of the simplest possible ligands, water, have proven rather difficult. For instance, calculations performed within the hybrid-GGA approximation with the B3LYP functional yielded a $^{55}Mn$ isotropic HFCC $A_{iso} = -164$ MHz, which is rather far from the experimental value (−245 MHz).[13] The same authors found that the sign of the experimental $^{17}O$ $A_{iso}$ value is well reproduced by calculations, but its magnitude is overestimated by 50%. Subsequent studies performed by Kaupp[14] and Neese[15] with the use of different functionals also provided calculated $^{17}O$ $A_{iso}$ values significantly larger than the experimental data.

The $^{17}O$ relaxation properties of the $[Mn(H_2O)_6]^{2+}$ complex were investigated by Merbach *et al.* at low magnetic field (1.4 T),[16] while $^1H$ Nuclear Magnetic Relaxation Dispersion (NMRD) profiles at a single temperature (308 K) were recorded by Bertini and co.[10] In this article, we present a combined experimental and computational study that aims at gaining information on the hyperfine coupling constants that govern the scalar contribution to $^1H$ relaxivity and the $^{17}O$ NMR chemical shifts and relaxation rates in $[Mn(H_2O)_6]^{2+}$. For this purpose, $^1H$ NMRD profiles were recorded at three different temperatures, while $^{17}O$ NMR chemical shifts and transverse relaxation times were measured at high magnetic field (11.7 T). DFT calculations and molecular dynamics studies based on the Atom Centered Density Matrix Propagation (ADMP) model were performed to gain information on the $A_O/\hbar$ and $A_H/\hbar$ hyperfine coupling constants and the relation between their values and the solution structure and dynamics of the complex.

**Experimental**

The proton $1/T_1$ NMRD profiles were measured on a fast field-cycling Stelar SmartTracer relaxometer (Mede, Pv, Italy) over a continuum of magnetic field strengths from 0.00024 to 0.25 T (corresponding to 0.01–10 MHz proton Larmor frequencies). The relaxometer operates under computer control with an absolute uncertainty in $1/T_1$ of ±1%. The temperature was controlled with a Stelar VTC-91 airflow heater equipped with a calibrated copper–constantan thermocouple (uncertainty of ±0.1 K). Additional data points in the range 15–70 MHz were obtained on a Stelar Relaxometer equipped with a Bruker WP80 NMR electromagnet adapted to variable-field measurements (15–80 MHz proton Larmor frequency). For these $^1$H data a 3.2 mM solution of $Mn(NO_3)_2$ in non-deuterated water at pH = 1.7 was utilized. The exact complex concentration was determined by the BMS shift method at 11.7 T.[17] $^{17}$O NMR measurements were recorded on a Bruker Avance III spectrometer (11.7 T) equipped with a 5 mm probe and standard temperature control unit. A 8.4 mM aqueous solution of $[Mn(H_2O)_6]^{2+}$containing 2.0% of the $^{17}$O isotope (Cambridge Isotope) was used. The observed transverse relaxation rates were calculated from the signal width at half-height.

Computational methods

All calculations presented in this work were performed employing the Gaussian 09 package (Revision B.01).[18] Full geometry optimizations of the $[Mn(H_2O)_6]^{2+}$ system were performed employing DFT within the hybrid *meta*-GGA approximation with the TPSSh exchange-correlation functional.[19] For geometry optimization purposes, we used the standard Ahlrichs' valence double-ξ basis set including polarization functions (SVP).[20] Geometry optimizations of the $[Mn(H_2O)_6]^{2+}$ system were also performed using the more extended Ahlrichs' valence triple-ξ basis set including polarization functions (TZVP).[21] The calculated Mn–O distances calculated at the TPSSh/SVP and TPSSh/TZVP levels differ by only 0.01 Å. Convergence of geometry optimizations of the $[Mn(H_2O)_6]^{2+}$ complex in aqueous solution were found to be problematic, while for the $[Mn(H_2O)_6]^{2+}\cdot 12H_2O$ system convergence was achieved. No symmetry constraints have been imposed during the optimizations. The highest spin state was considered as the ground state (sextuplet, $3d^5$). Since these calculations were performed by using an unrestricted model, spin contamination[22] was assessed by a comparison of the expected difference between $S(S + 1)$ for the assigned spin state ($S(S + 1) = 8.75$) and the actual value of $\langle S^2 \rangle$.[23] The results obtained indicate that spin contamination is negligible for systems investigated in this work [$\langle S^2 \rangle - S(S + 1) < 0.0040$]. The stationary points found on the potential energy surfaces as a result of geometry optimizations were tested to represent energy minima rather than saddle points *via* frequency analysis. The default values for the integration grid (75 radial shells and 302 angular points) and the SCF energy convergence criteria ($10^{-8}$) were used in all calculations.

Classical trajectory calculations of $[Mn(H_2O)_6]^{2+}$ and $[Mn(H_2O)_6]^{2+}\cdot 12H_2O$ were performed in aqueous solution at the TPSSh/SVP level by using the Atom Centered Density Matrix Propagation (ADMP) molecular dynamics model.[24] Time steps of 0.2 fs were used during the simulations and a total of 5000 steps were run for the trajectory simulations. The fictitious electron mass was 0.1 amu. All the ADMP calculations were started from the corresponding optimized geometries obtained as described above.

Isotropic $^{17}$O, $^1$H and $^{55}$Mn HFCCs in the $[Mn(H_2O)_6]^{2+}$ and $[Mn(H_2O)_6]^{2+}\cdot 12H_2O$ systems were calculated in aqueous solution with unrestricted DFT methods by employing the TPSSh exchange-correlation functional. For the description of H and O we used the EPR-III basis sets of Barone,[25] which is a triple-zeta basis set including diffuse functions, double d-polarizations and a single set of f-polarization functions, together with an improved s-part to better describe the nuclear region. For Mn we used the aug-cc-pVTZ-J basis set developed by Sauer for the calculation of EPR HFCCs, which is described by a (25s17p10d3f2g)/[17s10p7d3f2g] contraction scheme, and contains four tight s-, one tight p-, and one tight d-type function.[26] In the case of the $[Mn(H_2O)_6]^{2+}$ system, test calculations were also performed employing five additional functionals within the LSDA (SVWN[27,28]), GGA (BLYP[29,30]), *meta*-GGA (TPSS[19]), hybrid-

GGA (B3LYP[30,31]) and hybrid *meta*-GGA (M06[32]) approximations. The CAM-B3LYP hybrid functional, a long range corrected version of B3LYP using the Coulomb-attenuating method, was also tested.[33]

Throughout this work solvent effects were included by using the polarizable continuum model (PCM), in which the solute cavity is built as an envelope of spheres centered on atoms or atomic groups with appropriate radii. In particular, we used the integral equation formalism (IEFPCM) variant as implemented in Gaussian 09.[34]

## Results and discussion

### NMRD and $^{17}$O NMR studies

The increase of the water proton $R_1$ value, normalized to a 1 mM concentration of the paramagnetic species, is called relaxivity ($r_{1p}$) and it represents the efficiency of the paramagnetic solute in catalyzing the solvent relaxation at a given frequency and temperature. The relaxivity observed for $[Mn(H_2O)_6]^{2+}$ is the result of both inner- and outer-sphere contributions. The inner sphere term ($r_{1is}$) is given in eqn (1), where $q$ is the number of inner sphere water molecules ($q$ = 6 for $[Mn(H_2O)_6]^{2+}$) and $\tau_m$ is the residence time of water protons in the inner coordination sphere.[35]

$$r_{1\mathrm{is}} = \frac{1}{1000} \times \frac{q}{55.55} \times \frac{1}{T_{1\mathrm{m}}^{\mathrm{H}} + \tau_{\mathrm{m}}} \qquad (1)$$

The longitudinal relaxation rate of inner sphere protons in $Mn^{II}$complexes, $1/T^{H}_{1m}$, can be split into the dipolar ($1/T^{DD}_{1m}$) and scalar or Fermi contact term ($1/T^{SC}_{1m}$).[36] The dipolar contribution is the result of the modulation of the dipolar interaction between the electron (metal-based) and nuclear (of the bound water molecules) magnetic moments. The modulation occurs through rotation of the complex ($\tau_R$), electron magnetic moment relaxation ($T_{1,2e}$) and chemical exchange of the coordinated water molecules with bulk water ($k_{ex} = 1/\tau_M$). The enhancement of $R_1$ also depends on the number ($q$) of bound water molecules and their distance ($r_{MnH}$) from the metal centre, and on the applied magnetic field strength (eqn (2) and (3)):

$$\frac{1}{T_{1\mathrm{m}}^{\mathrm{DD}}} = \frac{2}{15}\left(\frac{\mu_0}{4\pi}\right)\frac{^2\gamma_I{}^2 g^2 \mu_B{}^2}{r_{\mathrm{MnH}}{}^6} S(S+1)\left[\frac{3\tau_{\mathrm{d1}}}{1+\omega_{\mathrm{I}}{}^2\tau_{\mathrm{d1}}{}^2} + \frac{7\tau_{\mathrm{d2}}}{1+\omega_{\mathrm{S}}{}^2\tau_{\mathrm{d2}}{}^2}\right] \qquad (2)$$

$$\frac{1}{\tau_{\mathrm{di}}} = \frac{1}{\tau_{\mathrm{m}}} + \frac{1}{\tau_{\mathrm{R}}} + \frac{1}{T_{\mathrm{ie}}} \quad i = 1,2 \qquad (3)$$

where $\omega_I$ is the proton resonance frequency and $\omega_S$ is the Larmor frequency of the $Mn^{II}$ electron spin. It has been reported that the scalar contribution to $^1$H relaxivity (eqn (4)) is responsible for a non-negligible part of the inner-sphere contribution to relaxivity in a few $Mn^{II}$ complexes such as $[Mn(H_2O)_6]^{2+}$ and $[Mn_2(ENOTA)(H_2O)_2]$.[9,10]

$$\frac{1}{T_1^{SC}} = \frac{2S(S+1)}{3}\left(\frac{A_H}{\hbar}\right)^2\left(\tau_{s1} + \frac{\tau_{s2}}{1+\tau_{s2}{}^2\omega_s{}^2}\right) \quad (4)$$

Here $A_H/\hbar$ represents the $^1$H hyperfine or scalar coupling constant and $1/\tau_{si}$ is the sum of the exchange rate constant and the longitudinal ($1/T_{1e}$) or transverse ($1/T_{2e}$) electron spin relaxation rates:

$$\frac{1}{\tau_{si}} = \frac{1}{\tau_m} + \frac{1}{T_{ie}} \quad (5)$$

The outer-sphere contribution to relaxivity arises from solvent molecules diffusing in the vicinity of the paramagnetic complex, and depends on additional parameters: the relative diffusion coefficient of solute and solvent molecules, $D$, and their distance of closest approach, $a$.[37]

The temperature dependence of $^{17}$O transverse relaxation rates ($R_2$) is given by the Swift–Connick equations,[38] which depend primarily on $T_{1,2e}$, the hyperfine coupling constant $A_O/\hbar$, $\tau_M$ and $q$ (eqn (6)–(9)):

$$\frac{1}{T_{2r}} = \frac{1}{\tau_m}\frac{T_{2m}{}^{-2}+\tau_m{}^{-1}T_{2m}{}^{-2}+\Delta\omega_m{}^2}{\left(\tau_m{}^{-1}+T_{2m}{}^{-1}\right)^2+\Delta\omega_m{}^2} \quad (6)$$

$$\Delta\omega_r = \frac{1}{P_m}(\omega - \omega_A) = \frac{\Delta\omega_m}{\left(1+\tau_m T_{2m}{}^{-1}\right)^2+\tau_m{}^2\Delta\omega_m{}^2} \quad (7)$$

$$\Delta\omega_m = \frac{g_L\mu_B S(S+1)B}{3k_B T}\frac{A_O}{\hbar} \quad (8)$$

$$\frac{1}{T_{2m}} \cong \frac{1}{T_{2sc}} = \frac{S(S+1)}{3}\left(\frac{A_O}{\hbar}\right)^2\left(\tau_{s1} + \frac{\tau_{s2}}{1+\tau_{s2}{}^2\omega_s{}^2}\right) \quad (9)$$

In these eqn (1)/$T_2$ and $\omega$ are the measured $^{17}$O NMR transverse relaxation rates and angular frequencies of the paramagnetic solution, $1/T_{2A}$ and $\omega_A$ the corresponding values of the acidified water reference, $1/T_{2r}$ and $\Delta\omega_r$ represent the reduced relaxation rates and reduced chemical shifts, $1/T_{2m}$ is the relaxation rate of the bound water, $\Delta\omega_m$ is the chemical shift difference between bound and bulk water and $P_m$ is the mole fraction of the bound water.

Nuclear magnetic relaxation dispersion (NMRD) profiles of $[Mn(H_2O)_6]^{2+}$were measured at 283, 298 and 310 K in the proton Larmor frequency range 0.01–70 MHz, corresponding to magnetic field strengths varying between $2.343 \times 10^{-4}$ and 1.645 T (Fig. 1). The relaxivity of $[Mn(H_2O)_6]^{2+}$decreases with increasing temperature in the proton Larmor frequency range 0.1–70 MHz, which shows that the relaxivity is limited by

the fast rotation of the complex in solution rather than by a slow water exchange rate. As usually observed for small $Mn^{II}$ chelates,[3–5] the NMRD profiles show a dispersion between 2 and 20 MHz. In addition, a second dispersion occurs between 0.5 and 0.02 MHz. This has been previously observed by Bertini *et al.* in the NMRD profile recorded at 308 K,[10] and attributed to an important scalar contribution to proton relaxivity.

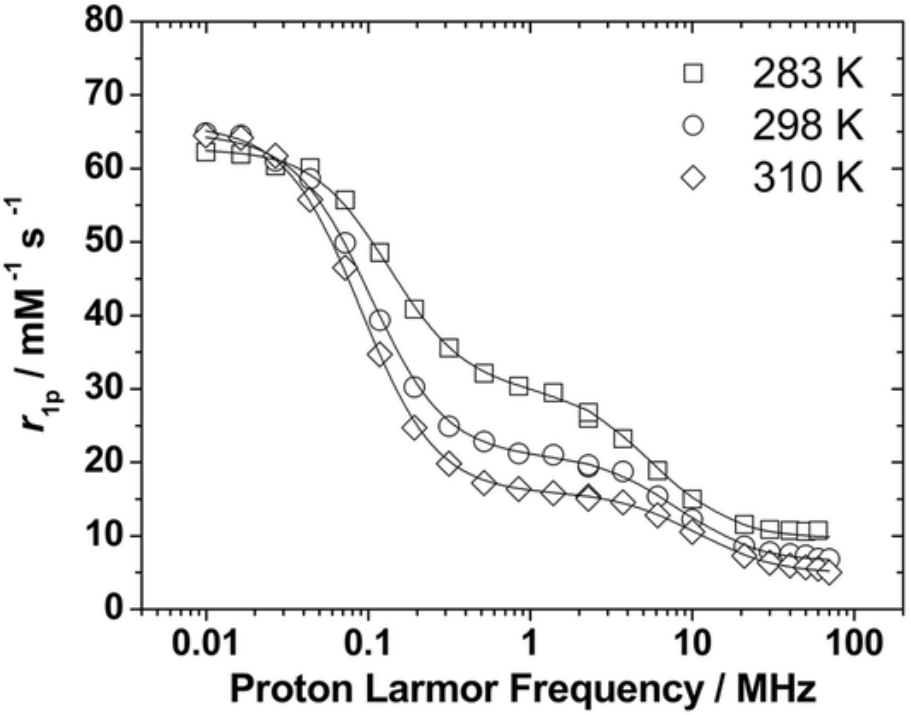


**Fig. 1.** $^{1}$H NMRD profiles recorded at different temperatures for $[Mn(H_2O)_6]^{2+}$ at pH 1.7. The lines represent the fit of the data as explained in the text.

The reduced transverse $^{17}$O relaxation rates and chemical shifts measured for $[Mn(H_2O)_6]^{2+}$ are presented in Fig. 2. Although the full eqn (6) was used to fit the experimental $^{17}$O NMR data, it is useful to consider the simplified eqn (10), in which the contribution to $1/T_{2r}$ of the chemical shift difference between the bound and bulk water ($\Delta\omega_m$) has been neglected.

$$\frac{1}{T_{2r}} \cong \frac{1}{\tau_m + T_{2m}} \qquad (10)$$

The sign of the temperature dependence of $1/T_{2r}$ depends on whether the transverse relaxation is dominated by $\tau_M$, which decreases with increasing temperature, or by the relaxation time of the bound water molecule, $T_{2m}$, which normally increases with increasing temperature. For $[Mn(H_2O)_6]^{2+}$ $1/T_{2r}$ increases with decreasing temperature below 357 K, reaches a maximum around 312 K, and then decreases in the temperature range 312–275 K. The maximum observed in the temperature dependence of $1/T_{2r}$ is therefore indicative of a changeover from the fast exchange regime at high temperatures, where $T_{2m}$ is the dominant term in eqn (10), to the low exchange regime at low temperatures, where $\tau_M$ is the dominant term.[39] The changeover between fast and slow exchange is also manifested in the temperature dependence of $\Delta\omega_r$, which shows an inflection point corresponding to the maximum in $1/T_{2r}$. Most of the $Mn^{II}$ complexes studied so far

do not show a maximum in the temperature dependence of $1/T_{2r}$, or this maximum is observed at lower temperatures in comparison with $[Mn(H_2O)_6]^{2+}$ (*i.e.* $[Mn(CyDTA)(H_2O)]^{2-}$).[40] These qualitative observations point to a relatively long residence time of the inner-sphere water molecules in the aqua-ion.

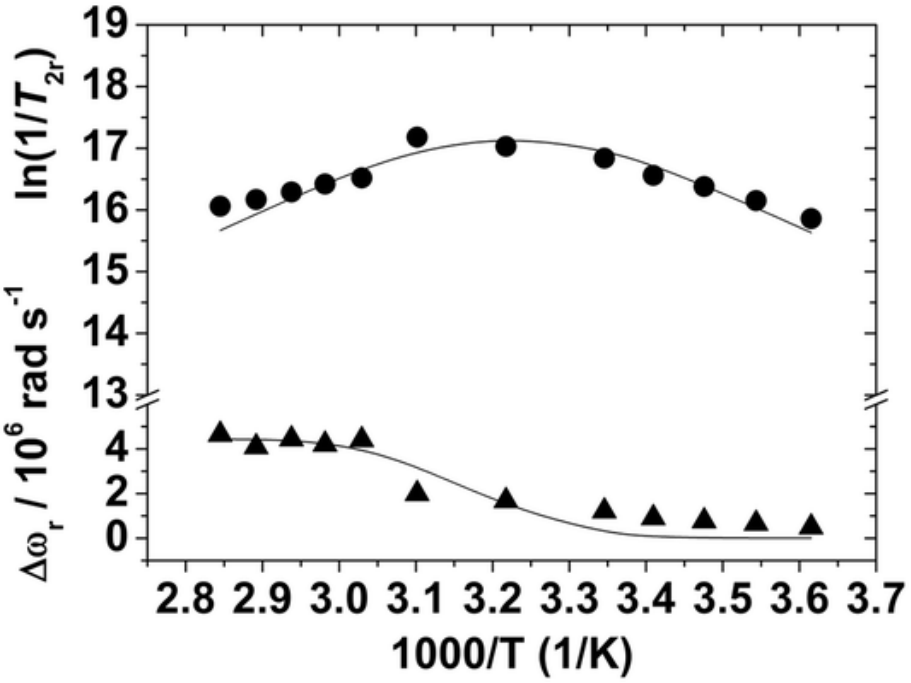


**Fig. 2.** Reduced transverse (●) $^{17}O$ relaxation rates and $^{17}O$ chemical shifts (▲) measured at 11.74 T for $[Mn(H_2O)_6]^{2+}$ (pH 1.7). The lines represent the fit of the data as explained in the text.

A simultaneous analysis of the NMRD and $^{17}O$ NMR data of $[Mn(H_2O)_6]^{2+}$gave the parameters listed in Table 1, while the curve fits are shown in Fig. 1 and 2. Some parameters were fixed during the fitting procedure: the distance of closest approach for the outer-sphere contribution $a_{MnH}$ was fixed at 3.6 Å, while the distance between the proton nuclei of the coordinated water molecule and the $Mn^{II}$ ion ($r_{MnH}$) was fixed at 2.83 Å. The number of water molecules in the inner coordination sphere of $Mn^{II}$was fixed to $q$ = 6, while the value of the diffusion coefficient, $D_{MnH}^{298}$, was fixed to the value of the self-diffusion coefficient of water molecules in pure water ($D_{MnH}^{298}$ = 2.3 × $10^{-9}$ $m^2$ $s^{-1}$).[41] The values of $a_{MnH}$ and $D_{MnH}^{298}$ used in the analysis of the data were taken on the basis of the data reported in the literature for different $Mn^{II}$ complexes.[3–5] It is worth noting that the outer-sphere contribution to relaxivity is relatively small for $[Mn(H_2O)_6]^{2+}$ (Fig. S1, ESI[i]). As a result, an accurate determination of these parameters from the analysis of the NMRD data was not possible.

The water exchange rate determined for $[Mn(H_2O)_6]^{2+}$ ($k_{ex}^{298}$ = 28.2 × $10^6$± 3.5 $s^{-1}$) is very similar to that determined by Merbach *et al.* from $^{17}O$ NMR measurements at 1.4 T.[16] The water exchange rates determined for six- and seven-coordinated $Mn^{II}$ complexes are faster than that of the fully aquated species (see for instance the data given in Table 1 for $[Mn(EDTA)(H_2O)]^{2-}$and [Mn(1,4-DO2A)($H_2O$)]). This effect has been attributed to the high-spin $d^5$ configuration, which does not have appreciable angular dependence on ligand field stabilization. Thus, despite the coordination of a ligand, conformational changes during the water substitution process are easily feasible in $d^5$ systems.[39]

**Table 1.** Parameters obtained from the simultaneous analysis of $^{17}O$ NMR and NMRD data of $[Mn(H_2O)]^{2+}$ and reference $Mn^{II}$ complexes.[a]

| Parameter | $[Mn(H_2O)_6]^{2+}$ | $[Mn(EDTA)]^{2-}$ | [Mn(1,4-DO2A)] |
|---|---|---|---|
| $k_{ex}^{298}/10^6$ s$^{-1}$ | 28.2 ± 3.5 | 471 | 1134 |
| $\Delta H^{\ddagger}$ kJ mol$^{-1}$ | 45.6 ± 3.5 | 33.5 | 29.4 |
| $\tau_R^{298}$/ps | 30.0 ± 0.2 | 57 | 46 |
| $E_r$/kJ mol$^{-1}$ | 16.7 ± 1.8 | 21.8 | 19.1 |
| $\tau_V^{298}$/ps | 10.0 ± 10.0 | 27.9 | 4.4 |
| $E_v$/kJ mol$^{-1}$ | 14.6 ± 0.7 | 1.0 | 1.0 |
| $D_{MnH}^{298}/10^{-10}$ m$^2$ s$^{-1}$ | 23.0 | 23.1 | 23.0 |
| $E_{DMnH}$/kJ mol$^{-1}$ | 29.7 ± 9.6 | 18.9 | 17.3 |
| $\Delta^2/10^{19}$ s$^{-2}$ | 0.06 ± 0.06 | 6.9 | 48.1 |
| $A_O/\hbar/10^6$ rad s$^{-1}$[b] | −34.6 ± 1.6 | −40.5 | −43.0 |
| $A_H/\hbar/10^6$ rad s$^{-1}$ | 5.43 ± 0.03 | 0.0 | 0.0 |
| $r_{MnH}$/Å | 2.83 | 2.83 | 2.83 |
| $a_{MnH}$/Å | 3.6 | 3.6 | 3.6 |
| $q^{298}$ | 6 | 1 | 0.87 |

[a] Italicized values were fixed during the fitting procedures. [b] There is some confusion about the sign of the $^{17}O$ isotropic HFCC in $Mn^{II}$ complexes. In contrast to recent experimental work, the correct sign of $A_O/\hbar = 2\pi A_{iso}$ of a water molecule bound to $Mn^{II}$ is negative, and corresponds to negative spin densities at the point of nucleus that causes an upfield shift of the $^{17}O$ resonance.

The $\tau_R^{298}$ value obtained from the analysis of the $^1H$ NMRD profiles (30.0 ps) is somewhat shorter than those determined for small $Mn^{II}$ complexes such as $[Mn(EDTA)(H_2O)]^{2-}$ and [Mn(1,4-DO2A)($H_2O$)], in line with the lower molecular weight of the aquated species. The quality of the fits was found to be quite insensitive to the parameters determining the electron spin relaxation $\Delta^2$ and $\tau_V$, and therefore the fitted parameters present rather large errors. However, the activation energy for the modulation of the zero-field-splitting ($E_V$), which was obtained with a very small statistical error, is in very good agreement with the value obtained from EPR measurements (10.5 kJ mol$^{-1}$).[42]

The hyperfine coupling constant $A_O/\hbar$ determined for $[Mn(H_2O)_6]^{2+}$($-34.6 \times 10^6$ rad s$^{-1}$) is in the low part of the range typically observed for $Mn^{II}$ complexes ($-32 \times 10^6$ to $-43 \times 10^6$ rad s$^{-1}$).[43] A $A_O/\hbar$ HFCC of $-34.6 \times 10^6$ rad s$^{-1}$ corresponds to a $A_{iso}$ value of −5.5 MHz, which is considerably smaller than that determined with ENDOR spectroscopy from frozen solution (−7.5 MHz).[13] The $^1H$ HFCC $A_H/\hbar$ was found to be $5.5 \times 10^6$ rad s$^{-1}$, which corresponds to a $A_{iso}$ value of 0.86 MHz. The only $Mn^{II}$ complex for which $A_H/\hbar$ could be determined from $^1H$ relaxation data, $[Mn_2(ENOTA)(H_2O)_2]$, presents a somewhat lower $A_H/\hbar$ HFCC ($2.9 \times 10^6$ rad s$^{-1}$).[9]

DFT calculations on the $[Mn(H_2O)_6]^{2+}$ and $[Mn(H_2O)_6]^{2+}\cdot 12H_2O$ systems

As expected, the geometry of $[Mn(H_2O)_6]^{2+}$ optimized at the TPSSh/SVP level presents an octahedral geometry according to the Mn–O bonds, with the overall molecule having a $T_d$ symmetry (Fig. 3). The calculated Mn–O distance (2.194 Å), is in good agreement with those observed in the solid state with X-ray crystallography,[44] and that determined from EXAFS spectra at 25 °C (2.17 Å).[45] Different computational studies provided similar geometries with Mn–O bond distances in the range 2.20–2.25 Å.[46]

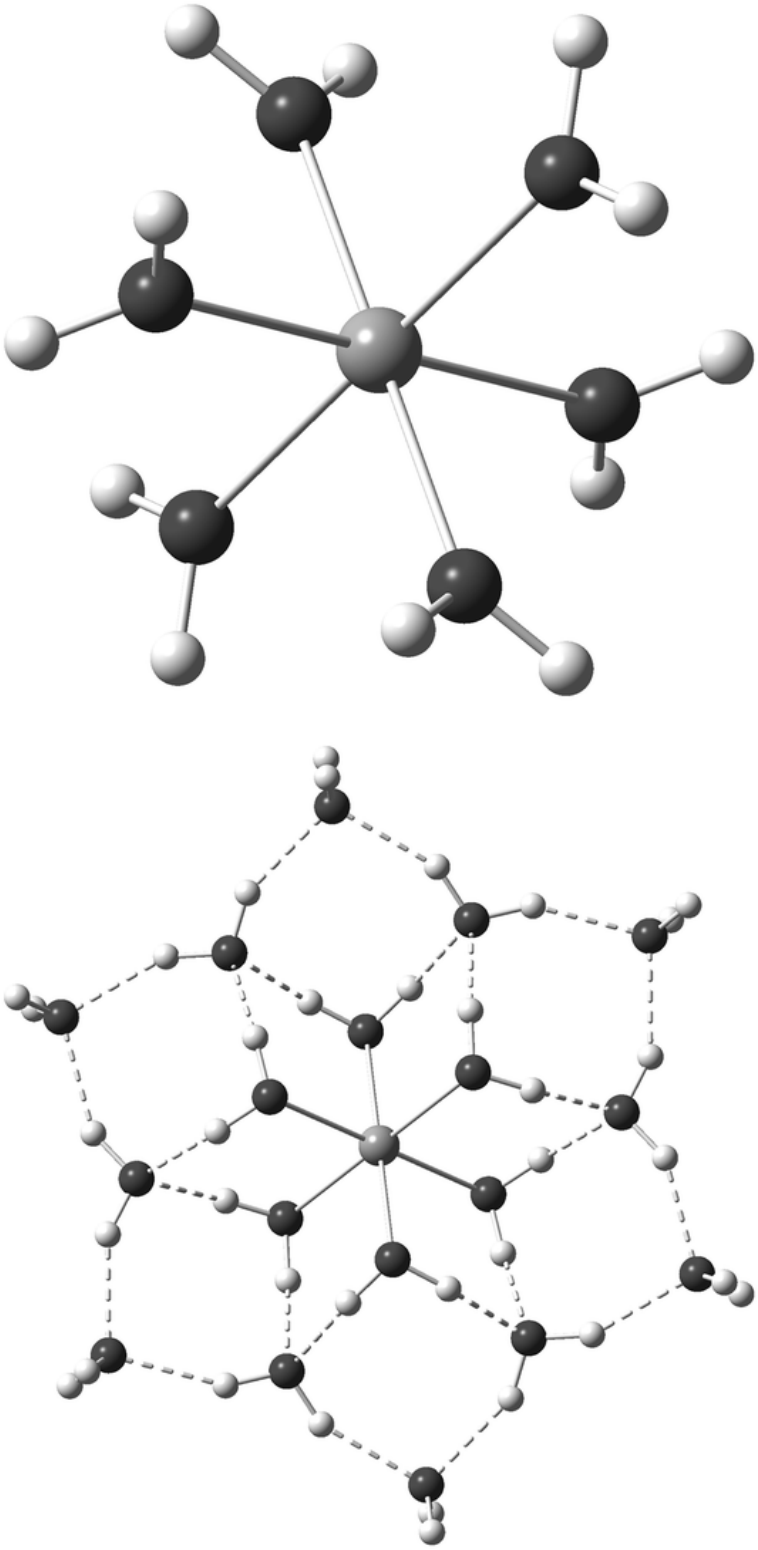

**Fig. 3.** Geometries of the $[Mn(H_2O)_6]^{2+}$ (top) and $[Mn(H_2O)_6]^{2+}\cdot 12H_2O$ (bottom) systems optimized at the TPSSh/SVP level.

The hyperfine coupling tensor for the nucleus *N* consists of three contributions, namely the isotropic Fermi contact (FC) and the anisotropic spin-dipolar contributions and the spin-orbit contribution. The isotropic FC contribution ($A_{iso}$) is given by:[47]

$$A_{\mathrm{iso}}(N) = \frac{4\pi}{3S}\beta_{\mathrm{e}}\beta_{\mathrm{N}}g_{\mathrm{e}}g_{\mathrm{N}}\rho^{\alpha-\beta}(R_{\mathrm{N}}) \qquad (11)$$

where $\beta_N$ and $\beta_e$ are the nuclear and Bohr magnetons, respectively, $g_N$ and $g_e$ are nuclear and free-electron $g$ values, $S$ is the total electron spin of the system, and $\rho^{\alpha-\beta}(R_N)$ represents the difference between majority spin ($\alpha$) and minority spin ($\beta$) densities at the position of the nucleus $N$.

Calculations of the $^{1}$H, $^{17}$O and $^{55}$Mn HFCCs in $[Mn(H_2O)_6]^{2+}$ were performed using single point calculations in aqueous solution on the optimized geometry described above. The data reported in Table 2 indicate that the SVWN, B3LYP, TPSS, M06, TPSSh and CAM-B3LYP functionals provide $^{1}$H and $^{17}$O HFCCs in good mutual agreement, while the GGA functional BLYP provides somewhat larger absolute values for both $^{1}$H and $^{17}$O $A_{iso}$. Among all the functionals tested in this work on the $[Mn(H_2O)_6]^{2+}$system the hybrid *meta*-GGA functional TPSSh provides the best overall agreement with the experimental $^{1}$H, $^{17}$O and $^{55}$Mn $A_{iso}$ values. Even so, the TPSSh functional gives calculated HFFCs that deviate up to 30% with respect to the values obtained with field ENDOR measurements in frozen solution[13] and up to 90% ($^{17}$O) and 70% ($^{1}$H) with respect with the values obtained from the analysis of the NMRD and $^{17}$O NMR data.

**Table 2.** $^{17}$O, $^{1}$H and $^{55}$Mn hyperfine coupling constants ($A_{iso}$, MHz) calculated for $[Mn(H_2O)_6]^{2+}$ and $[Mn(H_2O)_6]^{2+}\cdot 12H_2O$.

| | Functional | $^{17}$O | $^{1}$H | $^{55}$Mn |
|---|---|---|---|---|
| $[Mn(H_2O)_6]^{2+}$ | SVWN | −10.45 | 1.36 | −141.7 |
| | BLYP | −12.57 | 1.83 | −131.1 |
| | B3LYP | −10.73 | 1.39 | −159.8 |
| | TPSS | −10.68 | 1.68 | −175.5 |
| | M06 | −10.04 | 1.16 | −0.81 |
| | CAM-B3LYP | −10.25 | 1.27 | −162.7 |
| | TPSSh | −9.90 | 1.47 | −189.9 |
| $[Mn(H_2O)_6]^{2+}\cdot 12H_2O$ | TPSSh[a] | −6.97 | 0.69 | −173.9 |
| | TPSSh[b] | −7.05 | 0.75 | −172.5 |
| Experimental | | −7.5[c] | | −245[c] |
| | | −5.4[d] | 0.86[d] | |

[a] Data obtained from the equilibrium geometry.
[b] Calculated values obtained from the analysis of the trajectories of ADMP simulations (see text).
[c] Obtained from high field ENDOR measurements in frozen solutions, ref. 13.
[d] Obtained in this work from a simultaneous fitting of the NMRD and $^{17}$O NMR chemical shifts and relaxation rates.

In previous works we have shown that the explicit inclusion of a few second-sphere water molecules was crucial to obtain accurate $^{17}$O and $^{1}$H HFCCs in both $Mn^{II}$ and $Gd^{III}$ complexes.[3,4,48] Thus, we have performed calculations using a cluster–continuum approach explicitly including twelve second-sphere water molecules. This approach may be used to overcome the deficiency of continuum solvent models to account for specific hydrogen-bonding interactions involving inner-sphere and second-sphere water molecules. Twelve is the number of second-sphere water molecules expected to interact by hydrogen bonding to the six coordinated water molecules, and therefore clusters with formula $[M(H_2O)_6]^{2+}\cdot 12H_2O$ have been extensively investigated with *ab initio* and DFT calculations to gain information on the arrangement of first- and second-sphere water

molecules in different metal aqua-complexes.[49] The structure of the $[Mn(H_2O)_6]^{2+}\cdot 12H_2O$ system optimized in aqueous solution at the TPSSh/SVP level possesses a slightly distorted $S_6$ symmetry. In our model six second-sphere water molecules present Mn···O distances of 3.734 Å, and are involved in hydrogen-bonding interactions with two coordinated water molecules occupying *cis* positions in the octahedral coordination polyhedron. These second sphere water molecules are bridged *via* hydrogen bonds by a second set of second-sphere water molecules with Mn···O distances of 5.257 Å. The calculated Mn–O distance (2.215 Å) is in excellent agreement with the experimental values obtained both in the solid state and in solution.[44,45]

The $^{1}H$ and $^{17}O$ values calculated for the $[Mn(H_2O)_6]^{2+}\cdot 12H_2O$ system (Table 2) are considerably closer to the experimental values determined by ENDOR spectroscopy,[13] as well as to those obtained in this work from NMRD and $^{17}O$ NMR measurements. This reflects the importance of introducing the most important interactions involving the first and second hydration shells to compute accurate HFCCs in aqueous solution.

ADMP molecular dynamics simulations

Dynamic effects might have an important impact on the $^{1}H$, $^{17}O$ and $^{55}Mn$ $A_{iso}$ values, as the HFCCs measured are weighted averages ($\langle A_{iso} \rangle$) of individual values for the different configurations present in the sample. Among the different molecular dynamics methods available, we have chosen the atom-centered density matrix propagation (ADMP) approach, which provides O(*N*) scaling of computational time with system size, *N*being the number of electrons,[50] making it a reasonable choice compared to other computationally more expensive *ab initio* molecular dynamics methods.

ADMP simulations were performed in aqueous solution at the TPSSh/SVP level, and started on the equilibrium geometries of the $[Mn(H_2O)_6]^{2+}$ and $[Mn(H_2O)_6]^{2+}\cdot 12H_2O$ systems. The overall simulation time was 1 ps. The calculations performed on the $[Mn(H_2O)_6]^{2+}$ system resulted in the de-coordination of one of the inner-sphere water molecules during the course of the simulation in the time range 0.4–0.6 ps. The mean residence time of a coordinated water molecule in the $[Mn(H_2O)_6]^{2+}$ complex was determined to be ∼4 ns from the analysis of the NMRD and $^{17}O$ NMR data described above. However, no water exchange events were observed during the simulations performed on the $[Mn(H_2O)_6]^{2+}\cdot 12H_2O$ system, which again highlights the importance of treating explicitly the second-sphere solvation shell for an adequate description of the $Mn^{II}$ aqua-ion.

The calculations performed on the $[Mn(H_2O)_6]^{2+}\cdot 12H_2O$ system (Fig. 4) indicate that the octahedral coordination environment suffers relatively important distortions during the length of the simulations. These distortions affect the individual Mn–O bond distances, which fluctuate between 2.03 and 2.46 Å, and the individual *trans* O–Mn–O angles of the octahedral coordination polyhedron, which take a value of 180° in the equilibrium geometry and reach values as low as 165.5° during the simulation. The mean distortion of the octahedral coordination polyhedron was assessed by calculating $\Delta d_{Mn-O}$ and $\sigma$ defined as:

$$\Delta d_{\mathrm{Mn-O}} = \sum_{i=1}^{6} (d_{\mathrm{Mn-O}})_i - (d_{\mathrm{Mn-O}})_0 \qquad (12)$$

$$\sigma = \sum_{i=1}^{3} (180 - \sigma_i) \qquad (13)$$

where $(d_{Mn-O})_i$ accounts for the six Mn–O distances at each point of the simulation, $(d_{Mn-O})_0$ represents the distance observed in the equilibrium geometry (2.215 Å) and $\sigma_i$ represents each of the three *trans* O–Mn–O

angles of the octahedral coordination polyhedron. The $\Delta d_{Mn-O}$ parameter oscillates between +0.044 and −0.018, with a significant longer portion of the simulation showing positive values. This indicates that dynamic effects result in an effective lengthening of the Mn–O distances. Parameter $\sigma$ takes a value of 0.0° at the beginning of the simulation and reaches a maximum value of 10.3° during the length of the simulation. Thus, both the average Mn–O distances and O–Mn–O angles change significantly during the course of the ADMP simulations.

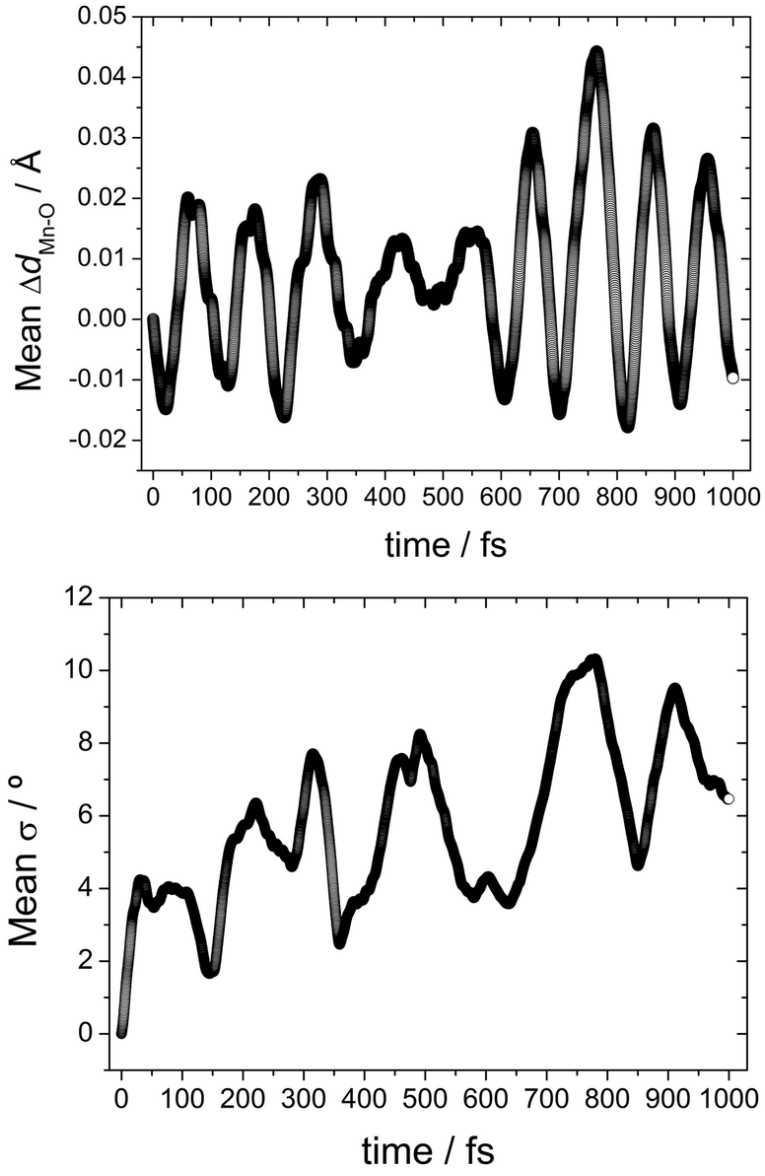


**Fig. 4.** Calculated mean $\Delta d_{Mn-O}$ distances and mean σ angles (σ = 180 – θ, where θ denotes trans O–Mn–O angles of the octahedral polyhedron) during the full length of the ADMP simulations performed in aqueous solution on the $[Mn(H_2O)_6]^{2+}\cdot 12H_2O$ system.

The trajectories obtained from ADMP simulations were used to perform a configurational space sampling by taking 100 snapshots at regular intervals of 10 fs. The $^{1}H$, $^{17}O$ and $^{55}Mn$ $A_{iso}$ values were subsequently calculated for each snapshot. The average $A_{iso}$ values ( $\langle A_{iso} \rangle$ ) obtained for the 100 configurations are shown in Table 2. Thus, $\langle A_{iso} \rangle$ were calculated as the average of 100, 600 and 1200 individual $A_{iso}$ values for $^{55}Mn$, $^{17}O$ and $^{1}H$, respectively. Our results indicate that dynamic effects have a negligible effect on

the $^{17}O$ and $^{55}Mn$ HFCCs (<1.2%), while the mean $A_{iso}$ value of the lighter $^{1}H$ nucleus increases by *ca.* 8% while approaching the experimental value.

Although the mean $A_{iso}$ values obtained from ADMP simulations do not differ significantly from those obtained for the equilibrium geometry, the individual $^{17}O$ and $^{1}H$ $A_{iso}$ values for a given water molecule change markedly during the simulation. This allows correlating the calculated HFCCs with geometrical parameters, thereby providing information on the factors that affect the magnitude of the HFCCs. In previous works we have shown that the $^{17}O$ HFCCs of coordinated water molecules in $Gd^{III}$ and $Mn^{II}$ complexes are significantly affected by changes in the M–O bond distances and the orientation of the water molecule plane with respect to the metal–O vector.[4,48] Plots of the calculated $^{17}O$ $A_{iso}$ values *versus* the Mn–O distance and the Mn–O–H–H dihedral angle indeed show linear trends (Fig. 5), thereby confirming our previous findings.

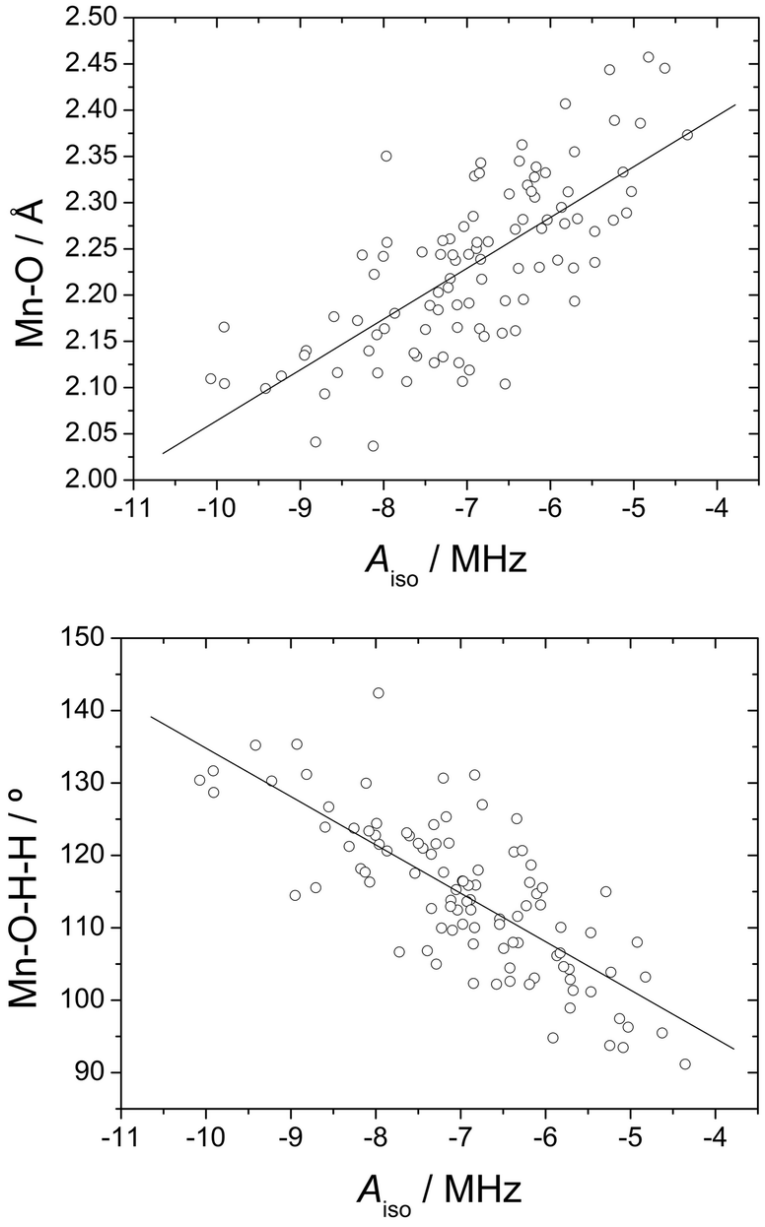


**Fig. 5.** $^{17}O$ isotropic hyperfine coupling constant, $A_{iso}$, plotted as function of Mn–$O_W$ distance (top) and the Mn–O–H–H dihedral angle (bottom) for 100 configurations extracted from MD trajectory calculations on the $[Mn(H_2O)_6]^{2+}\cdot 12H_2O$ system.

The $A_{iso}$ values obtained from ADMP trajectory calculations were fitted to the following expression:

$$A_{\mathrm{iso}}\left(^{17}\mathrm{O}\right) = a_0 + a_1(1/r_{\mathrm{MnO}}) + a_2\phi \qquad (14)$$

where $r_{MnO}$ is the Mn–O distance (in Å), $\phi$ is the Mn–O–H–H dihedral angle and $a_0$, $a_1$ and $a_2$ are fitting parameters. The best fit of the data provided $a_0$ = 16.1 ± 1.3 MHz, $a_1$ = −34.2 ± 3.0 MHz Å and $a_2$ = −0.067 ± 0.005 MHz deg$^{-1}$. The $A_{iso}$ values obtained with eqn (14) for each of the snapshots show a reasonably good linear correlation with those obtained with DFT (Fig. 6), which confirms that the Mn–O bond distances and the orientation of the water molecule plane with respect to the metal–O vector are the main factors affecting the $^{17}$O $A_{iso}$ values. The mean Mn–O distance of the 100 configurations used to calculate the $^{17}$O $A_{iso}$ values amounts to 2.234 Å, which is somewhat longer than that determined experimentally with EXAFS (2.17 Å).[45] The tilt angle between the Mn–O axis and the plane of the water molecules in $[Mn(H_2O)_6]^{2+}$ was determined to be 110 ± 15°.[51] The average value obtained from the data shown in Fig. 5 amounts to 114°, in good agreement with the experiment.

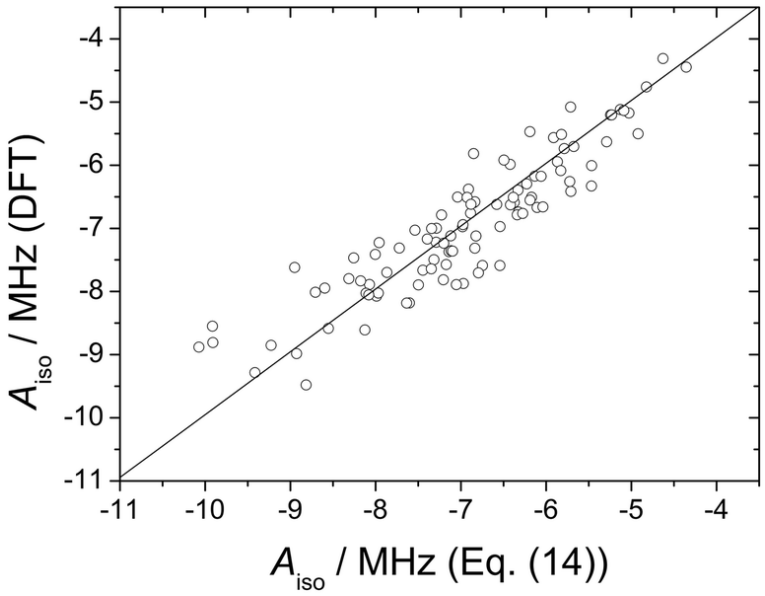


**Fig. 6.** $^{17}$O isotropic hyperfine coupling constant obtained from DFT calculations on 100 configurations extracted from MD trajectory calculations on the $[Mn(H_2O)_6]^{2+}\cdot 12H_2O$ system plotted against those obtained with eqn (14) ($R^2$ = 0.91).

Both the Mn–O distance and the dihedral $\phi$ angle are expected to change significantly depending upon the $Mn^{II}$ coordination environment. For instance, the Mn–$O_{water}$ distance in different $Mn^{II}$ complexes containing inner-sphere water molecules were found to vary in the range 2.19–2.30 Å.[9,43g] Regarding the tilt angle of the coordinated water molecule, it has been estimated to fall within the range 90–145° for $Gd^{III}$ complexes.[52] By constraining the $r_{MnO}$ and $\phi$ values within these ranges, eqn (14) provides $^{17}$O $A_{iso}$ values in the range −4.8 to −9.2 MHz, which correspond to $A_O/\hbar$values of 30–58 × 10$^6$ rad s$^{-1}$. This simple estimate suggests that the $^{17}$O HFCCs of coordinated water molecules in $Mn^{II}$ complexes may differ significantly depending on the particular structure of the complex.

The $^{1}$H HFCCs (Fig. 7) calculated for each of the 100 snapshots extracted from the trajectory calculations correlate reasonably well with the corresponding $^{17}$O $A_{iso}$ values, which indicates that both $^{1}$H and $^{17}$O HFCCs are affected in a similar way by the Mn–$O_W$ distances and Mn–O–H–H dihedral angles. While the $^{17}$O $A_{iso}$ values are negative, $^{1}$H $A_{iso}$ values are positive. However, these different signs correspond to positive spin densities at the point nucleus of both $^{17}$O and $^{1}$H, due to the different sign of the magnetic moment of these nuclei. This confirms that both the $^{1}$H and $^{17}$O HFCCs are dominated by the spin delocalization mechanism rather than by spin polarization effects.[4]

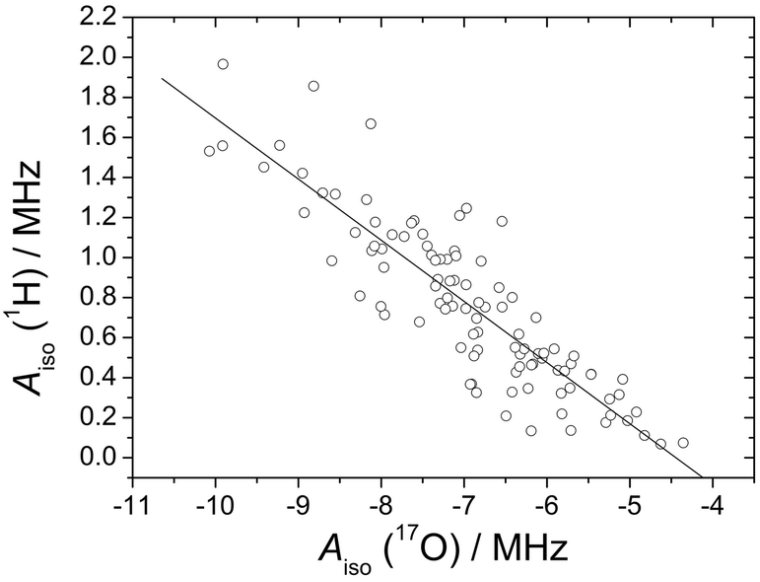


**Fig. 7.** $^{17}$O isotropic hyperfine coupling constant plotted as function of the $^{1}$H hyperfine coupling constant for 100 configurations extracted from MD trajectories of $[Mn(H_2O)_6]^{2+}\cdot 12H_2O$ ($R^2 = 0.82$)

The scalar contribution to $^{1}$H relaxivity

As discussed above, the NMRD profiles of $[Mn(H_2O)_6]^{2+}$ indicate an important scalar contribution to $^{1}$H relaxivity, which is accounted for by eqn (4). However, only one $Mn^{II}$ chelate has been reported to date to possess a significant scalar contribution to relaxivity,[9] which is generally assumed to be dominated by the dipolar mechanism. To understand the role of the scalar contribution to relaxivity, we have performed simulations in which $1/T^{SC}_1$ is plotted as a function of the water exchange rate and transverse electron spin relaxation rates (Fig. 8). The longitudinal and transverse electronic relaxation rates, $1/T_{1e}$ and $1/T_{2e}$, are often approximated by using eqn (15) and (16),[36] where $\tau_v$ is the electronic correlation time for the modulation of the zero-field-splitting interaction, $E_V$ the corresponding activation energy and $\Delta^2$ is the mean square zero-field-splitting energy.

$$\frac{1}{T_{1e}} = \frac{1}{25}\Delta^2\tau_V\{4S(S+1)-3\}\left(\frac{1}{1+\omega_s{}^2\tau_v{}^2}+\frac{4}{1+4\omega_s{}^2\tau_v{}^2}\right) \qquad (15)$$

$$\frac{1}{T_{2e}} = \frac{1}{50}\Delta^2\tau_V\{4S(S+1)-3\}\left(\frac{5}{1+\omega_s{}^2\tau_v{}^2}+\frac{2}{1+4\omega_s{}^2\tau_v{}^2}+3\right) \qquad (16)$$

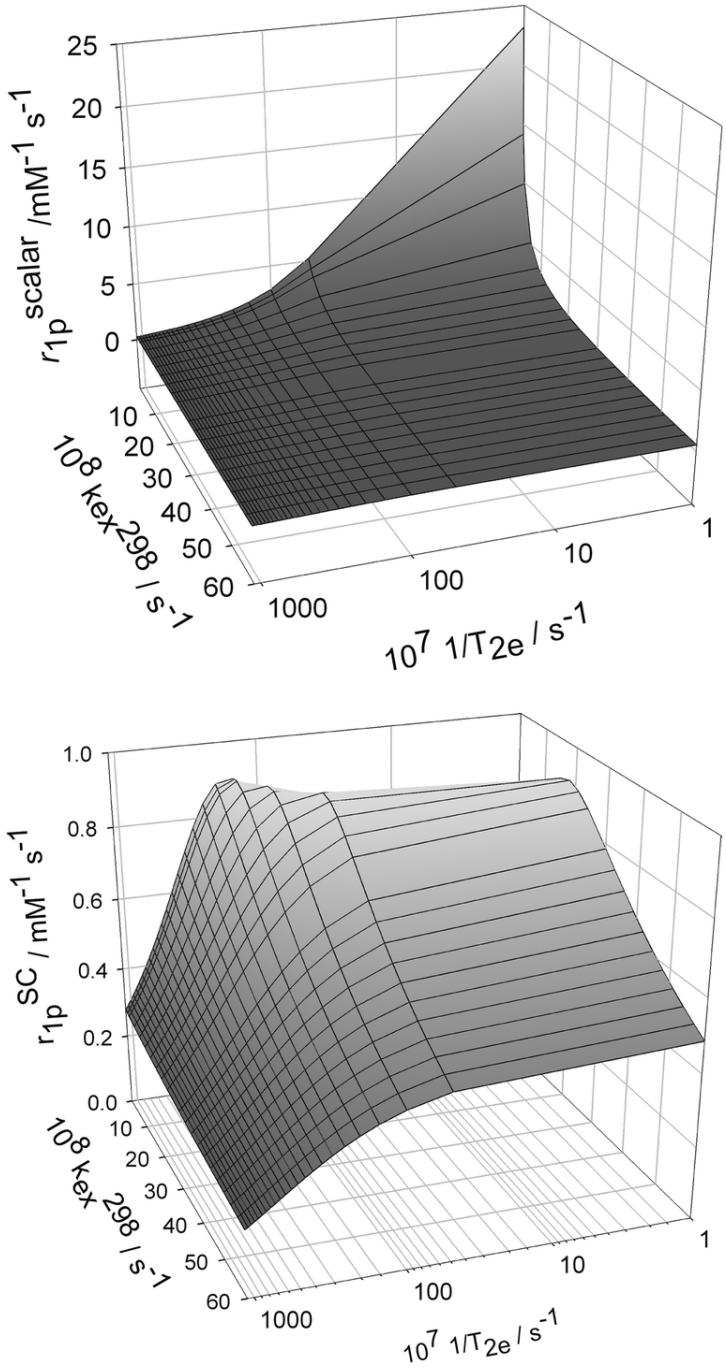


**Fig. 8.** Surface plots showing the calculated scalar contribution to relaxivity ($r^{SC}_{1p}$) as a function of the water exchange rate ($k_{ex}^{298}$) and the electron spin transverse electronic relaxation ($1/T_{2e}$). The following parameters were used for the simulations: $A_H/\hbar$ = 5.5 rad $s^{-1}$, q = 1, B = 0.0003 T (top) and B = 0.01 T (bottom). Note the logarithmic scale of the axis representing $1/T_{2e}$.

It has been shown that eqn (15) and (16) provide a rather crude approximation of the electron spin relaxation for $Gd^{III}$ complexes,[53] and it is likely that they are neither very accurate for $Mn^{II}$ compounds. However, they can still be used to analyze NMRD profiles even at low magnetic fields for small $Mn^{II}$ complexes.[43]

The simulations shown in Fig. 8 were obtained using two different magnetic fields (0.01 and 0.0003 T, corresponding to proton Larmor frequencies of 0.43 and 0.013 MHz, respectively) and eqn (1), (4), (5) and (16). The number of inner-sphere water molecules $q$ was taken as 1.0, as stable $Mn^{II}$-based contrast agents are expected to possess one (or perhaps 2) coordinated water molecules. The $^1H$ hyperfine

coupling constant ($A_H/\hbar$) was assumed to be equal to the value obtained for $[Mn(H_2O)_6]^{2+}$ ($5.4 \times 10^6$ rad $s^{-1}$, Table 1). A comparison of the relaxivities calculated at 0.01 and 0.003 T clearly shows that the scalar contribution to relaxivity drops quickly as the magnetic field increases. At low field, the calculated $r^{SC}_{1p}$ values are only significant for particularly slow electron spin relaxation rates ($1/T_{2e} < 5 \times 10^8$ $s^{-1}$). A slow electron spin relaxation explains the high scalar contribution to relaxivity observed for $[Mn(H_2O)_6]^{2+}$ (the values of $\tau_V$ and $\Delta^2$given in Table 1 give $1/T_{2e} = 3.9 \times 10^8$ $s^{-1}$ with the use of eqn (16)). On the contrary, $Mn^{II}$ complexes with poliaminocarboxylate ligands often show much faster electron relaxation ($1/T_{2e} = 6 \times 10^9$ to $3 \times 10^{10}$ $s^{-1}$).[3] The slower electronic relaxation of $[Mn(H_2O)_6]^{2+}$ in comparison with the $Mn^{II}$complexes investigated so far as potential MRI contrast agents is in line with the hyperfine splitting observed in the EPR spectrum of the aqua-ion,[42] which is however not observed for chelates as a result of line-broadening.[3] Concerning the effect of water exchange rate, at low field it is clear that the scalar contribution to relaxivity is only significant for small $k_{ex}$ values ($k_{ex}^{298} < 12 \times 10^8$ $s^{-1}$). Since the water exchange rates determined for $Mn^{II}$chelates are faster than that of the fully aquated species, it is not surprising that $Mn^{II}$ complexes lack a significant scalar contribution to relaxivity in most cases. We also notice that the water exchange rate determined for $[Mn_2(ENOTA)(H_2O)]$ ($5.5 \times 10^7$ $s^{-1}$), which presents a sizable scalar contribution, is very close to that of the aqua ion. Increasing the magnetic field results in a broader distribution of $k_{ex}^{298}$ and $1/T_{2e}$ values that give non-negligible scalar contributions (the observed relaxivity for small $Mn^{II}$complexes at *ca.* 0.01 T is around 4–5 $mM^{-1}$ $s^{-1}$ at 298 K). At this magnetic field the scalar contribution is also favoured by slow electron spin relaxation times and water exchange rates of *ca.* $k_{ex}^{298} = 15 \times 10^8$ $s^{-1}$.

## Conclusions

We have performed a $^1H$ and $^{17}O$ NMR relaxometric study of the $[Mn(H_2O)_6]^{2+}$ complex as well as a theoretical analysis of the $^1H$ and $^{17}O$ HFCCs of the coordinated water molecules in this system. Our DFT calculations show that the explicit inclusion of a second solvation shell is critical to obtain accurate HFCCs. Molecular dynamics simulations show that the $^1H$ and $^{17}O$ HFCCs on inner-sphere water molecules are very sensitive to the Mn–O distances and the orientation of the coordinated water molecule plane with respect to the Mn–O vector. However, the average HFCCs obtained from up to 100 snapshots extracted from trajectory calculations do not differ significantly from the corresponding $A_{iso}$ values obtained for the equilibrium geometries, and remain reasonably close to the experimental ones. The important scalar contribution to proton relaxivity in $[Mn(H_2O)_6]^{2+}$ is related to a slow electron spin relaxation and a rather slow water exchange rate of the inner-sphere water molecules.

## Acknowledgements

D. E.-G. thanks Xunta de Galicia (EM2012/088) for generous financial support. C. P.-I. thanks Centro de Supercomputación de Galicia (CESGA) for providing the computer facilities. M. B. thanks the support by the Compagnia di San Paolo (Bando Ateneo-CSP 2012; Project: NANOPROGLY).

## Notes and references

1. I. Bertini and C. Luchinat, *Coord. Chem. Rev.*, 1996, **150**, 77.

2. F. Rastrelli and A. Bagno, *Chem. – Eur. J.*, 2009, **15**, 7990.

3. G. A. Rolla, C. Platas-Iglesias, M. Botta, L. Tei and L. Helm, *Inorg. Chem.*, 2013, **52**, 3268.

4. V. Patinec, G. A. Rolla, M. Botta, R. Tripier, D. Esteban-Gómez and C. Platas-Iglesias, *Inorg. Chem*., 2013, **52**, 11173.

5. (a) S. Aime, P. L. Anelli, M. Botta, M. Brochetta, S. Canton, F. Fedeli, E. Gianolio and E. Terreno, *J. Biol. Inorg. Chem.*, 2002, **7**, 58. (b) G. A. Rolla, L. Tei, M. Fekete, F. Arena, E. Gianolio and M. Botta, *Bioorg. Med. Chem*., 2011, **19**, 1115. (c) L. Tei, G. Gugliotta, M. Fekete, F. K. Kalman and M. Botta, *Dalton Trans*., 2011, **40**, 2025.

6. *The Chemistry of Contrast Agents in Medical Magnetic Resonance Imaging*, ed. A. E. Merbach, L. Helm and É. Tóth, Wiley, New York, 2nd ed., 2013.

7. B. Drahos, I. Lukes and E. Toth, *Eur. J. Inorg. Chem*., 2012, 1975.

8. D. H. Powell, O. M. Ni Dhubhghaill, D. Pubanz, L. Helm, Y. S. Lebedev, W. Schlaepfer and A. E. Merbach, *J. Am. Chem. Soc*., 1996, **118**, 9333.

9. E. Balogh, Z. He, W. Hsieh, S. Liu and E. Toth, *Inorg. Chem*., 2007, **46**, 238.

10. I. Bertini, F. Briganti, Z. Xia and C. Luchinat, *J. Magn. Reson*., 1993, **101**, 198.

11. O. Schiemann, J. Frischer, N. Kisseleva, S. T. Sigurdsson and T. F. Prisner, *ChemBioChem*, 2003, **4**, 1057.

12. (a) J. Schraut, A. V. Arbuznikov, S. Schinzel and M. Kaupp, *ChemPhysChem*, 2011, **12**, 3170. (b) N. Cox, W. Ames, B. Epel, L. V. Kulik, L. Rapatskiy, F. Neese, J. Messinger, K. Wieghardt and W. Lubitz, *Inorg. Chem*., 2011, **50**, 8238.

13. D. Baute and D. Goldfarb, *J. Phys. Chem. A*, 2005, **109**, 7865.

14. S. Schinzel, R. Müller and M. Kaupp, *Theor. Chem. Acc*., 2008, **120**, 437.

15. S. Kossmann, B. Kirchner and F. Neese, *Mol. Phys*., 2007, **105**, 2049.

16. Y. Ducommun, K. E. Newman and A. E. Merbach, *Inorg. Chem*., 1980, **19**, 3696.

17. D. M. Corsi, C. Platas-Iglesias, H. van Bekkum and J. A. Peters, *Magn. Reson. Chem*., 2001, **39**, 723.

18. M. J.Frisch, G. W.Trucks, H. B.Schlegel, G. E.Scuseria, M. A.Robb, J. R.Cheeseman, G.Scalmani, V.Barone, B.Mennucci, G. A.Petersson, H.Nakatsuji, M.Caricato, X.Li, H. P.Hratchian, A. F.Izmaylov, J.Bloino, G.Zheng, J. L.Sonnenberg, M.Hada, M.Ehara, K.Toyota, R.Fukuda, J.Hasegawa, M.Ishida, T.Nakajima, Y.Honda, O.Kitao, H.Nakai, T.Vreven, J. A.Montgomery, Jr, J. E.Peralta, F.Ogliaro, M.Bearpark, J. J.Heyd, E.Brothers, K. N.Kudin, V. N.Staroverov, R.Kobayashi, J.Normand, K.Raghavachari, A.Rendell, J. C.Burant, S. S.Iyengar, J.Tomasi, M.Cossi, N.Rega, J. M.Millam, M.Klene, J. E.Knox, J. B.Cross, V.Bakken, C.Adamo, J.Jaramillo, R.Gomperts, R. E.Stratmann, O.Yazyev, A. J.Austin, R.Cammi, C.Pomelli, J. W.Ochterski, R. L.Martin, K.Morokuma, V. G.Zakrzewski, G. A.Voth, P.Salvador, J. J.Dannenberg, S.Dapprich, A. D.Daniels, Ö.Farkas, J. B.Foresman, J. V.Ortiz, J.Cioslowski and D. J.Fox, *Gaussian 09, Revision B.1*, Gaussian, Inc., Wallingford CT, 2009.

19. J. M. Tao, J. P. Perdew, V. N. Staroverov and G. E. Scuseria, *Phys. Rev. Lett*., 2003, **91**, 146401.

20. A. Schaefer, H. Horn and R. Ahlrichs, *J. Chem. Phys*., 1992, **97**, 2571.

21. A. Schaefer, C. Huber and R. Ahlrichs, *J. Chem. Phys*., 1994, **100**, 5829.

22. J. F. Stanton and J. Gauss, *Adv. Chem. Phys*., 2003, **125**, 101.

23. A. Montoya, T. N. Truong and A. F. Sarofim, *J. Phys. Chem. A*, 2000, **124**, 6108.

24. (a) S. S. Iyengar, H. B. Schlegel, J. M. Millam, G. A. Voth, G. E. Scuseria and M. J. Frisch, *J. Chem. Phys.*, 2001, **115**, 10291. (b) H. B. Schlegel, J. M. Millam, S. S. Iyengar, G. A. Voth, G. E. Scuseria, A. D. Daniels and M. J. Frisch, *J. Chem. Phys*., 2001, **114**, 9758. (c) H. B. Schlegel, S. S. Iyengar, X. Li, J. M. Millam, G. A. Voth, G. E. Scuseria and M. J. Frisch, *J. Chem. Phys*., 2002, **117**, 8694.

25. N. Rega, M. Cossi and V. Barone, *J. Chem. Phys*., 1996, **105**, 11060.

26. E. D. Hedegard, J. Kongsted and S. P. A. Sauer, *J. Chem. Theory Comput*., 2011, **7**, 4077.

27. J. C. Slater, *The Self-Consistent Field for Molecular and Solids, Quantum Theory of Molecular and Solids*, McGraw-Hill, New York, 1974, vol. 4.

28. S. H. Vosko, L. Wilk and M. Nusair, *Can. J. Phys*., 1980, **58**, 1200.

29. A. D. Becke, *Phys. Rev. A*, 1988, **38**, 3098.

30. C. Lee, W. Yang and R. G. Parr, *Phys. Rev. B: Condens. Matter Mater. Phys*., 1988, **37**, 785.

31. A. D. Becke, *J. Chem. Phys.*, 1993, **98**, 5648.

32. Y. Zhao and D. G. Truhlar, *Theor. Chem. Acc*., 2008, **120**, 215.

33. T. Yanai, D. Tew and N. Handy, *Chem. Phys. Lett*., 2004, **393**, 51.

34. J. Tomasi, B. Mennucci and R. Cammi, *Chem. Rev*., 2005, **105**, 2999.

35. Z. Luz and S. Meiboom, *J. Chem. Phys*., 1964, **40**, 2686.

36. (a) I. Solomon, *Phys. Rev*., 1955, **99**, 559. (b) I. Solomon and N. Bloembergen, *J. Chem. Phys*., 1956, **25**, 261. (c) N. Bloembergen, *J. Chem. Phys*., 1957, **27**, 572. (d) N. Bloembergen and L. O. Morgan, *J. Chem. Phys.*, 1961, **34**, 842.

37. J. H. Freed, *J. Chem. Phys.*, 1978, **68**, 4034.

38. (a) T. J. Swift and R. E. Connick, *J. Chem. Phys*., 1962, **37**, 307. (b) T. J. Swift and R. E. Connick, *J. Chem. Phys.*, 1964, **41**, 2553.

39. J. Maigut, R. Meier, A. Zahl and R. van Eldik, *J. Am. Chem. Soc*., 2008, **130**, 14556.

40. J. Maigut, R. Meier, A. Zahl and R. van Eldik, *Inorg. Chem*., 2007, **47**, 5702.

41. R. Mills, *J. Phys. Chem*., 1973, **77**, 685.

42. A. W. Nolle and L. O. Morgan, *J. Chem. Phys*., 1962, **36**, 378.

43. (a) S. Aime, P. L. Anelli, M. Botta, M. Brochetta, S. Canton, F. Fedeli, E. Gianolio and E. Terreno, *J. Biol. Inorg. Chem.*, 2002, **7**, 58. (b) A. G. Rolla, L. Tei, M. Fekete, F. Arena, E. Gianolio and M. Botta, *Bioorg. Med. Chem*., 2011, **19**, 1115. (c) B. Drahos, J. Kotek, I. Cisarova, P. Hermann, L. Helm, I. Lukes and E. Toth, *Inorg. Chem*., 2011, **50**, 12785. (d) B. Drahos, M. Pniok, J. Havlickova, J. Kotek, I. Cisarova, P. Hermann, I. Lukes and E. Toth, *Dalton Trans*., 2011, **40**, 10131. (e) A. de Sa, C. S. Bonnet, C. F. G. C. Geraldes, E. Toth, P. M. T. Ferreira and J. P. Andre, *Dalton Trans*., 2013, **43**, 4522. (f) L.

Tei, G. Gugliotta, M. Fekete, F. K. Kalman and M. Botta, *Dalton Trans*., 2011, **40**, 2025. (g) B. Drahos, J. Kotek, P. Hermann, I. Lukes and E. Toth, *Inorg. Chem*., 2010, **49**, 3224.

44. F. A. Cotton, L. M. Daniels, C. A. Murillo and J. F. Quesada, *Inorg. Chem*., 1993, **32**, 4861.

45. Y. Chen, J. L. Fulton and W. Partenheimer, *J. Am. Chem. Soc*., 2005, **127**, 14085.

46. (a) H. A. de Abreu, L. Guimaraes and H. A. Duarte, *Int. J. Quantum Chem*., 2008, **108**, 2467. (b) F. P. Rotzinger, *J. Phys. Chem. B*, 2005, **109**, 1510.

47. F. Neese, *Coord. Chem. Rev*., 2009, **253**, 526.

48. D. Esteban-Gomez, A. de Blas, T. Rodriguez-Blas, L. Helm and C. Platas-Iglesias, *ChemPhysChem*, 2012, **13**, 3640.

49. (a) G. D. Markham, J. P. Glusker and C. W. Bock, *J. Phys. Chem. B*, 2002, **106**, 5118. (b) W. W. Rudolph and C. C. Pye, *J. Phys. Chem. A*, 2000, **104**, 1627. (c) J. Li, C. L. Fisher, J. L. Chen, D. Bashford and L. Noodleman, *Inorg. Chem*., 1996, **35**, 4694. (d) C. C. Pye and W. W. Rudolph, *J. Phys. Chem. A*, 1998, **102**, 9933. (e) C. W. Bock, G. D. Markham, A. K. Katz and J. P. Glusker, *Theor. Chem. Acc*., 2006, **115**, 100. (f) M. Pavlov, P. E. M. Siegbahn and M. Sandstrom, *J. Phys. Chem. A*, 1998, **102**, 219.

50. S. S. Iyengar, H. B. Schlegel and G. A. Voth, *J. Phys. Chem. A*, 2003, **107**, 7269.

51. G. W. Neilson, J. R. Newsome and M. Sandström, *J. Chem. Soc., Faraday Trans. 2*, 1981, **77**, 1245.

52. A. M. Raitsimring, A. V. Astashkin, D. Baute, D. Goldfarb and P. Caravan, *J. Phys. Chem. A*, 2004, **108**, 7318.

53. (a) A. Borel, S. Laus, A. Ozarowski, C. Gateau, A. Nonat, M. Mazzanti and L. Helm, *J. Phys. Chem. A*, 2007, **111**, 5399. (b) P. H. Fries, C. Gateau and M. Mazzanti, *J. Am. Chem. Soc*., 2005, **127**, 15801.

[i] Electronic supplementary information (ESI) available: Inner-sphere and outer-sphere contributions to relaxivity and optimized Cartesian coordinates obtained with DFT calculations. See DOI: 10.1039/c3ra45721d.